Article ID: 1006-8775(2024)01-0089-08

Fusion SST from Infrared and Microwave Measurement of FY-3D Meteorological Satellite

ZHANG Miao (张 淼)[1,2,3], XU Na (徐 娜)[1,2,3], CHEN Lin (陈 林)[1,2,3]

(1. National Satellite Meteorological Center/ National Center for Space Weather, Beijing 100081 China; 2. Innovation Center for Fengyun Meteorological Satellite (FYSIC), Beijing 100081 China; 3. Key Laboratory of Radiometric Calibration and Validation for Environmental Satellites, China Meteorological Administration, Beijing 100081 China)

Abstract: Sea surface temperature (SST) is one of the important parameters of global ocean and climate research, which can be retrieved by satellite infrared and passive microwave remote sensing instruments. While satellite infrared SST offers high spatial resolution, it is limited by cloud cover. On the other hand, passive microwave SST provides all-weather observation but suffers from poor spatial resolution and susceptibility to environmental factors such as rainfall, coastal effects, and high wind speeds. To achieve high-precision, comprehensive, and high-resolution SST data, it is essential to fuse infrared and microwave SST measurements. In this study, data from the Fengyun-3D (FY-3D) medium resolution spectral imager II (MERSI-II) SST and microwave imager (MWRI) SST were fused. Firstly, the accuracy of both MERSI-II SST and MWRI SST was verified, and the latter was bilinearly interpolated to match the 5km resolution grid of MERSI SST. After pretreatment and quality control of MERSI SST and MWRI SST, a Piece-Wise Regression method was employed to correct biases in MWRI SST. Subsequently, SST data were selected based on spatial resolution and accuracy within a 3-day window of the analysis date. Finally, an optimal interpolation method was applied to fuse the FY-3D MERSI-II SST and MWRI SST. The results demonstrated a significant improvement in spatial coverage compared to MERSI-II SST and MWRI SST. Furthermore, the fusion SST retained true spatial distribution details and exhibited an accuracy of –0.12±0.74°C compared to OSTIA SST. This study has improved the accuracy of FY satellite fusion SST products in China.

Key words: SST; data fusion; FY3; infrared; microwave

CLC number: P405 **Document code:** A

Citation: ZHANG Miao, XU Na, CHEN Lin. Fusion SST from Infrared and Microwave Measurement of FY-3D Meteorological Satellite [J]. Journal of Tropical Meteorology, 2024, 30(1): 89-96, https://doi.org/10.3724/j.1006-8775.2024.009

1 INTRODUCTION

Sea surface temperature (SST) is widely used in climate change monitoring, weather and ocean forecasting, national defense and military operations, ocean and atmospheric models, tourism, marine fisheries, and other fields [1-6]. However, SST observation based on ships and in situ methods is insufficient for large-scale real-time monitoring [7]. Satellite-based SST monitoring primarily utilizes infrared and microwave sensors [8-10], each with distinct advantages and limitations [11,12]. While infrared sensors offer high spatial resolution, they cannot retrieve SST data in the presence of cloud cover [13], resulting in limited SST coverage [14]. On the other hand, passive microwave sensors enable all-weather observation but suffer from poor spatial resolution and susceptibility to environmental factors such as rainfall, coastal effects, and high wind speeds [15]. Consequently, the fusion of SST data from both infrared and microwave sensors is essential to achieve a high-resolution, comprehensive, and accurate SST distribution field [16-18].

Early efforts by Chinese and international scholars in multi-satellite SST fusion have encompassed various fusion methods, including the stepwise revision method, mixed analysis method, OI method, three-dimensional variation method, and statistical optimal estimation method [19]. These efforts mainly focus on the fusion of foreign satellite SSTs, the main fusion products include: the optimum interpolation SST (OISST) V2.0 [20] developed by the National Oceanic and Atmospheric Administration (NOAA) National Climatic Data Center (NCDC) of the United States using the optimal interpolation (OI) method to fuse Advanced Very High Resolution Radiometer (AVHRR) and Advanced Microwave Scanning Radiometer (AMSR) data, the daily real-time global sea surface temperature-high resolution analysis (RTG-HR) SST [21] developed by the US NOAA National Centers for Environmental Prediction (NCEP) using the two-dimensional variational method to fuse the AVHRR and in-situ data, the operational sea surface temperature and sea ice analysis (OSTIA) SST [22] developed by the UK Met Office using the multi-scale OI technology to fuse the AVHRR, AMSR, MicrowaveImager

Received 2023-08-28; **Revised** 2023-11-15; **Accepted** 2024-02-15

Funding: Fengyun Satellite Application Advance Program (FY-APP-2021.0505)

Biography: ZHANG Miao, Senior Engineer, primarily undertaking research on satellite oceanography, retrieval and fusion of sea surface temperature from Fengyun satellite remote sensing.

Corresponding author: XU Na, e-mail: xuna@cma.gov.cn

(TMI), Advanced Long Track Scanning Radiometer (AATSR) and spinning enhanced visible and infrared imager (SEVIRI) data, the Canadian Meteorological Centre (CMC) SST [23] developed by the Canadian Meteorological Agency using OI technology to fuse AVHRR, Visible Infrared Imaging Radiometer Suite (VIIRS) and AMSR data. Some scholars have also made positive attempts to fuse Chinese satellite SST products. Qi and Lin [24] used the OI method to fuse Chinese marine satellite SST products, Miao et al. [25] used NOAA's Local Analysis Prediction System (LAPS) to fuse Chinese meteorological and marine satellite SST products, and Liao [26] used the OI method and the Kalman filtering method to reconstruct Chinese Fengyun-3C (FY-3C) SST data. However, none of these fusion products was published.

FY-3 satellites are China's second generation of polar orbit meteorological satellites [27]. FY-3A and FY-3B are experimental application satellites, and FY-3C, FY-3D, FY-3E, FY-3F, and FY-3G are operational satellites [28]. The operational satellites have successfully launched the morning orbit satellite FY-3C and FY-3F, the afternoon orbit satellite FY-3D, the early morning orbit satellite FY-3E and the inclined orbit satellite FY-3G. Medium resolution spectral imager II (MERSI-II) and microwave imager (MWRI) carried on the FY-3D can both realize the retrieval of SST. This paper mainly introduces the fusion algorithm and quality validation of FY-3D MERSI-II SST and MWRI SST.

2 DATASETS

2.1 *FY-3D/ MERSI-II SST*

FY-3D/MERSI-II SST uses the same statistical algorithm as FY-3C [29], and the retrieval model is shown in Eq. 1 and Eq. 2. The regression coefficient is obtained byregression calculation using the matching data of satellite observation brightness temperature and quality-controlled in-situ SST from the in-situ quality monitor (IQUAM) [30] under clear sky conditions.

$$T_s = a_0 + a_1 T_{11} + a_2 T_{FG}(T_{11} - T_{12}) + a_3(T_{11} - T_{12})(\sec\theta - 1) \quad (1)$$

$$T_s = a_0 + a_1 T_{11} + a_2 T_4 + a_3 T_{12} + a_4(T_4 - T_{12})(\sec\theta - 1) + a_5(\sec\theta - 1) \quad (2)$$

where T_s is the inverted SST, T_4, T_{11}, and T_{12} are respectively 3.8μm, 10.8μm and 12μm channel brightness temperature; a_0–a_5 are regression coefficients, θ is the zenith angle of the satellite, and T_{FG} is the first guess SST. This paper selects Copernicus Climate Change Service (C3S) V2.0 [31] as the first guess SST. Eq. 1 is a daytime algorithm, and Eq. 2 is a nighttime algorithm. The details of retrieval methods can be found in Wang et al. [29]. MERSI-II SST includes orbit products of 1km resolution and daily, ten-day, and monthly products of 5km resolution with quality flags. The pixels with the best quality flag are those whose zenith angle is less than 50 degrees, which has passed the spatial consistency test [29], and the absolute deviation is less than 2°C compared with C3S daily SST. Pixels with the best quality flag are selected for fusion.

2.2 *FY-3D/ MWRI SST*

FY-3D MWRI SST uses the same statistical algorithm as FY-3C [32], and the retrieval model is shown in Eq. 3 [33]. The regression coefficient is obtained by regression calculation using the matching samples of satellite observation brightness temperature and in-situ observation SST under non-rainfall conditions.

$$T_s = a_0 + \sum_{i=1}^{9}\left(a_i t_i + b_i t_i^2\right) \quad (3)$$

where T_s is the inverted SST. For 10.65, 18.7, and 36.5 GHz observed brightness temperature, $t_i = T_{Bi} - 150$, and for 23.8 GHz observed brightness temperature, $t_i = -\ln(290 - T_{Bi})$, where T_B is the MWRI observed brightness temperature at the corresponding frequency and polarization, and a and b are the regression coefficients. The details of the retrieval methods can be found in Zhang et al. [32]. MWRI SST includes orbit products of 10km resolution and daily, ten-day, and monthly products of 25km resolution with quality flags. The pixels with the quality flag of 50 have an absolute deviation of less than 1.5°C compared with the 30-year daily mean OISST from 1982 to 2011. Pixels with a quality flag of 50 are selected for fusion.

2.3 *OSTIA SST*

OSTIA SST fuses the in-situ, AVHRR, AMSR, TMI, AATSR, and SEVIRI SST data. All satellite SST data have been corrected using AATSR and in-situ SST [33]. It can provide near-real-time 5km resolution SST with an error of less than 0.3°C [34,35]. This study uses OSTIA SST as validation data.

3 METHOD

3.1 *Quality validation of FY-3D MERSI-II SST and MWRI SST*

The quality of the daily MERSI-II SST with the best quality flag and the daily MWRI SST with the quality flag of 50 are validated using the OSTIA data. MERSI-II SST and OSTIA SST have the same spatial resolution (5km); the difference between MERSI-II SST and OSTIA SST can be calculated directly by selecting the same grid point. For MWRI SST with a coarse spatial resolution (25km), the OSTIA SST in the MWRI grid is averaged and then calculated for error statistics.

Choose October 2020, January, April, and July 2021 to represent autumn, winter, spring, and summer, respectively. The daily error curve is shown in Fig. 1. The bias reflects the deviation between the retrieval and true values. In contrast, the root mean square error (RMSE) reflects the degree of dispersion between the retrieval value and the true value, which can better reflect the actual situation of the error [36]. Therefore, we

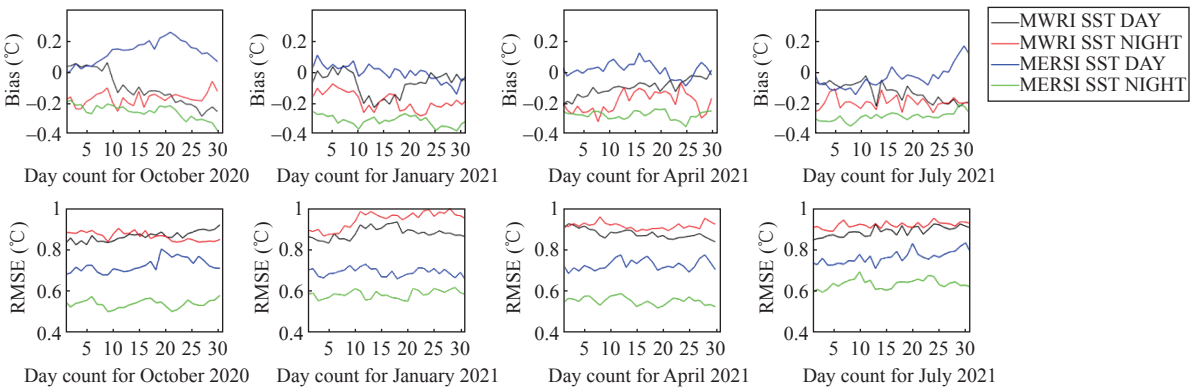

Figure 1. Daily error statistical curve of daily and nightly orbit synthesis MERSI SST and MWRI SST in October 2020, January, April, and July 2021.

prioritize the data source with a smaller RMSE during fusion. The error statistical results show that the accuracy of MERSI-II nighttime SST is –0.28±0.57°C, the accuracy of MERSI-II daytime SST is 0.02±0.72°C, the accuracy of MWRI daytime SST is –0.10±0.87°C, and the accuracy of MWRI nighttime SST is –0.18±0.91°C. The RMSE of MERSI-II SST is smaller than that of MWRI SST, mainly because the calibration accuracy of MERSI-II is better than that of MWRI [37,38]. The RMSE of infrared SST at night is less than that in the daytime, mainly because the 3.8 μm channel is not available in the daytime due to the influence of solar reflection and scattering. Still, the 3.8 μm channel is used at night, which is not sensitive to water vapor and is beneficial to improve the retrieval accuracy of infrared SST at night [29]. However, the RMSE of microwave SST in the daytime is less than that at night, mainly because the stability of MWRI ascending orbit (in the daytime) is better than that of descending orbit (in the night) [32].

3.2 *Bias correction of MWRI SST*

The quality validation results in Section 3.1 show that the RMSE of MWRI SST is significantly greater than that of MERSI-II SST. Therefore, to ensure the fusion SST's accuracy, this paper makes a bias correction for MWRI SST. The commonly used bias correction methods include Poisson's equation method, empirical orthogonal function and empirical orthogonal function telecorrelation method, probability density function method, Piece-Wise regression method, etc. [26]. In this study, the SST bias is corrected by the Piece-Wise regression method. This method establishes a regression model to match the associated in-situ SST with daily climatological SST, and the optimal match-ups are selected through the error analysis of the associated variables in the model; SSTs are then recalculated by using these optimal match-ups in the Piece-Wise regression model:

$$T_{\rm ds} = b_0 + b_1 T_s + b_2 (T_s - T_c) \tag{4}$$

where $T_{\rm ds}$ is the MWRI SST after bias correction, b_0–b_2 is the regression coefficient calculated from the optimal match-ups, T_s is the MWRI SST before bias correction, and T_c is the 30-year daily mean OISST. The details of the correction methods can be found in Liao [26].

It can be seen from Fig. 2 that the regions of MWRI SST with large bias after bias correction are significantly less than those before bias correction, and the overall bias is closer to 0°C in distribution. After bias correction, the pixel with an absolute deviation of less than 1.5°C compared with the 30-year daily mean OISST was also marked as 50. The proportion of samples with the quality flag of 50 to all ocean surfaces except sea ice before and after bias correction was 61.14% and 67.93%, respectively, and the proportion of samples with the quality flag of 50 after bias correction was increased by about 7%. Then, the

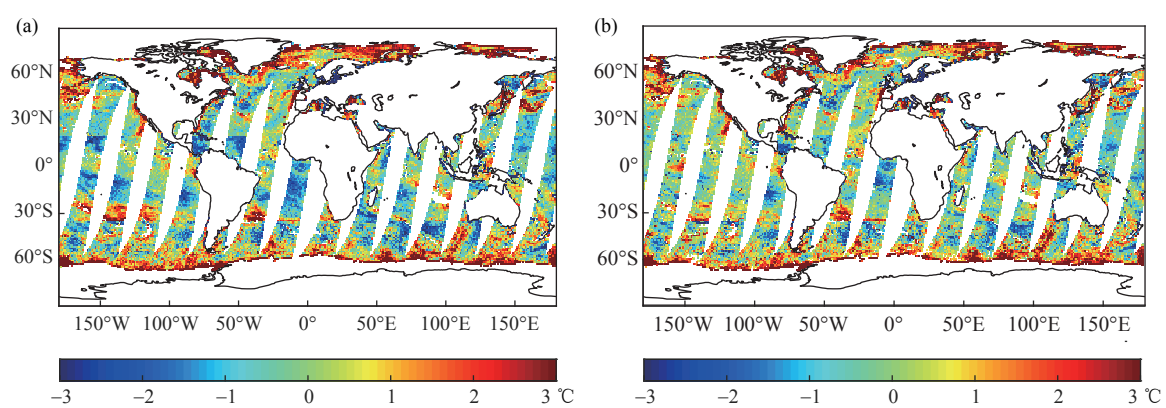

Figure 2. Difference distribution between OSTIA SST and MWRI SST (a) before bias correction and (b) after bias correction on 15 July, 2021.

quality of the MWRI SST after bias correction with the quality flag of 50 in October 2020, January, April, and July 2021 are validated using the OSTIA data. The daily error curve is shown in Fig. 3. The error statistical results show that the accuracy of the MWRI daytime SST after bias correction is 0±0.78°C, and the accuracy of MWRI nighttime SST after bias correction is –0.04±0.79°C. The bias after bias correction is significantly reduced compared with that before bias correction, and the RMSE is reduced by about 0.1K compared with that before bias correction.

3.3 *Fusion algorithm*

First, FY-3D/MERSI-II SST with a spatial resolution of 25km is bilinearly interpolated to the 5km resolution grid of MERSI-II SST. After pretreatment and quality control of MERSI-II SST and MWRI SST, a Piece-Wise Regression method is used for bias correction of MWRI SST; then the SST is selected in order of priority according to the spatial resolution and data accuracy using SST within 3 days of analysis date as follows: MERSI-II nighttime and daytime SST of analysis date, MERSI-II nighttime, and daytime SST of the previous day of analysis date, MERSI-II nighttime and daytime SST of previous two days of analysis date, MWRI daytime and nighttime SST of analysis date, MWRI daytime and nighttime SST of previous day of analysis date, MWRI daytime and nighttime SST of previous two days of analysis date. Then, the OI method is used to fuse the SST.

OI is an analysis method to minimize the variance of the analysis error estimated from the observation and background errors, assuming that the observation data and background field are unbiased estimates. In this method, the values on the spatial grid points are obtained by calculating the weights of the observed data and the background field, which makes the analysis error of the grid point to the minimum. The analysis increment at grid point k can be expressed as:

$$r_k = \sum_{i=1}^{N} w_{ik} q_i \tag{5}$$

where q_i is the observation increment at grid point i, obtained by subtracting the background field from the observation. N is the number of data. w_{ik} is the weight for q_i. The subscript k is the grid point in the analysis, and the subscripts i and j (used below) stand for the location of observation. Using Eq. 5, the analysis increments are calculated on the grid points; then, the SST analysis values can be obtained by adding the background values to them. In this study, the OSTIA SST at the previous time is selected as the background field.

If the analysis error, observation error, and background error of the grid point k are α_k, β_k, η_k respectively, then

$$q_i = \eta_i + \beta_i \tag{6}$$

$$a_k = r_k - \eta_k = \sum_{i=1}^{N} w_{ik} q_i - \eta_k \tag{7}$$

Substitute Eq. 7 into Eq. 6 and solve the variance sum of the analyzed SST field.

$$\sum_{k=1}^{N} (a_k)^2 = \sum_{k=1}^{N} \left[\sum_{i=1}^{N} w_{ik} (\eta_i + \beta_i) - \eta_k \right]^2 \tag{8}$$

w_{ik} can be solved by making the partial derivative of Eq. 8 with respect to w_{ik} (i=1, 2, ..., N; k=1, 2, ..., N), and making the partial derivative equal to zero. In this way, the following series of linear equations can be obtained:

$$\sum_{i=1}^{N} M_{ij} w_{ik} = \left\langle \eta_j \eta_k \right\rangle \tag{9}$$

where j=1, 2, …, N.

$$M_{ij} = \left\langle \eta_i \eta_j \right\rangle + \varepsilon_i \varepsilon_j \left\langle \beta_i \beta_j \right\rangle \tag{10}$$

In Eq. 10, $\left\langle \eta_i \eta_j \right\rangle$ is the mathematical expectation for the correlation error of the background field, $\left\langle \beta_i \beta_j \right\rangle$ is the mathematical expectation for the correlation error of the observation field, and ε is the noise-to-signal standard deviation ratio; here 0.5 is used. $\left\langle \eta_i \eta_j \right\rangle$ is assumed Gaussian, expressed as:

$$\left\langle \eta_i \eta_j \right\rangle = \exp\left[\frac{-(x_i - x_j)^2}{\lambda_x^2} + \frac{-(y_i - y_j)^2}{\lambda_y^2} \right] \tag{11}$$

where $x_i - x_j$ and $y_i - y_j$ are the zonal and meridional distance between grid i and j; λ_x and λ_y are the zonal and meridional scale parameters of correlation length; here, 150 km is used for both λ_x and λ_y.

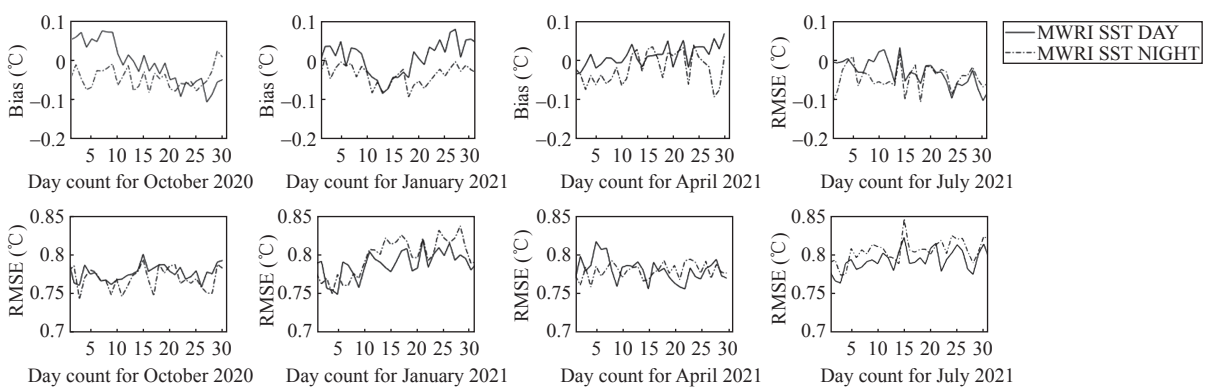

Figure 3. Daily error statistical curve of MWRI SST after bias correction in October 2020, January, April, and July 2021.

Assuming that the data errors are not correlated, then:

$$\langle \beta_i \beta_j \rangle = \delta_{ij} \quad (12)$$

For satellite data, it is assumed that the correlation and uncorrelation between data errors account for half respectively; then, $\langle \beta_i \beta_j \rangle = 0.5(\langle \eta_i \eta_j \rangle + \delta_{ij})$, where δ_{ij} =1 when i=j, and δ_{ij} =0 when i≠j.

4 RESULTS

It can be seen from Fig. 4 that MERSI-II SST has many areas without retrieval results due to the influence of clouds, with a space coverage rate of 44%. In contrast, MWRI SST has many blank areas between strips due to narrow width, with a space coverage rate of 55%, the space coverage of the fusion SST is significantly improved compared to MERSI-II SST and MWRI SST. Comparison between Fig. 4(c) and Fig. 4(d) shows that the fusion SST and the OSTIA SST have good consistency, and the fusion SST can retain the true spatial distribution details of SST. Due to cloud coverage in the Antarctic region, the fusion SST data mainly comes from the MWRI SST, while in the low SST region, the detection sensitivity of MWRI is reduced due to the lack of a 6.9 GHz channel [39], resulting in a high bias of SST [40].

The accuracy of the fusion SST on October 2020, January, April, and July 2021 are validated using OSTIA data. The results are shown in Fig. 5; it can be seen that the daily error of the fusion SST is basically stable, with an accuracy of –0.12±0.74°C (Table 1). The main reason for seasonal differences in fusion SST is that the SST data sources participating in the fusion have seasonal differences in spatial coverage and accuracy. Samples where the difference between fusion SST and OSTIA SST is less than ±1K account for more than 70% of the total, indicating that fusion SST and OSTIA SST have good consistency.

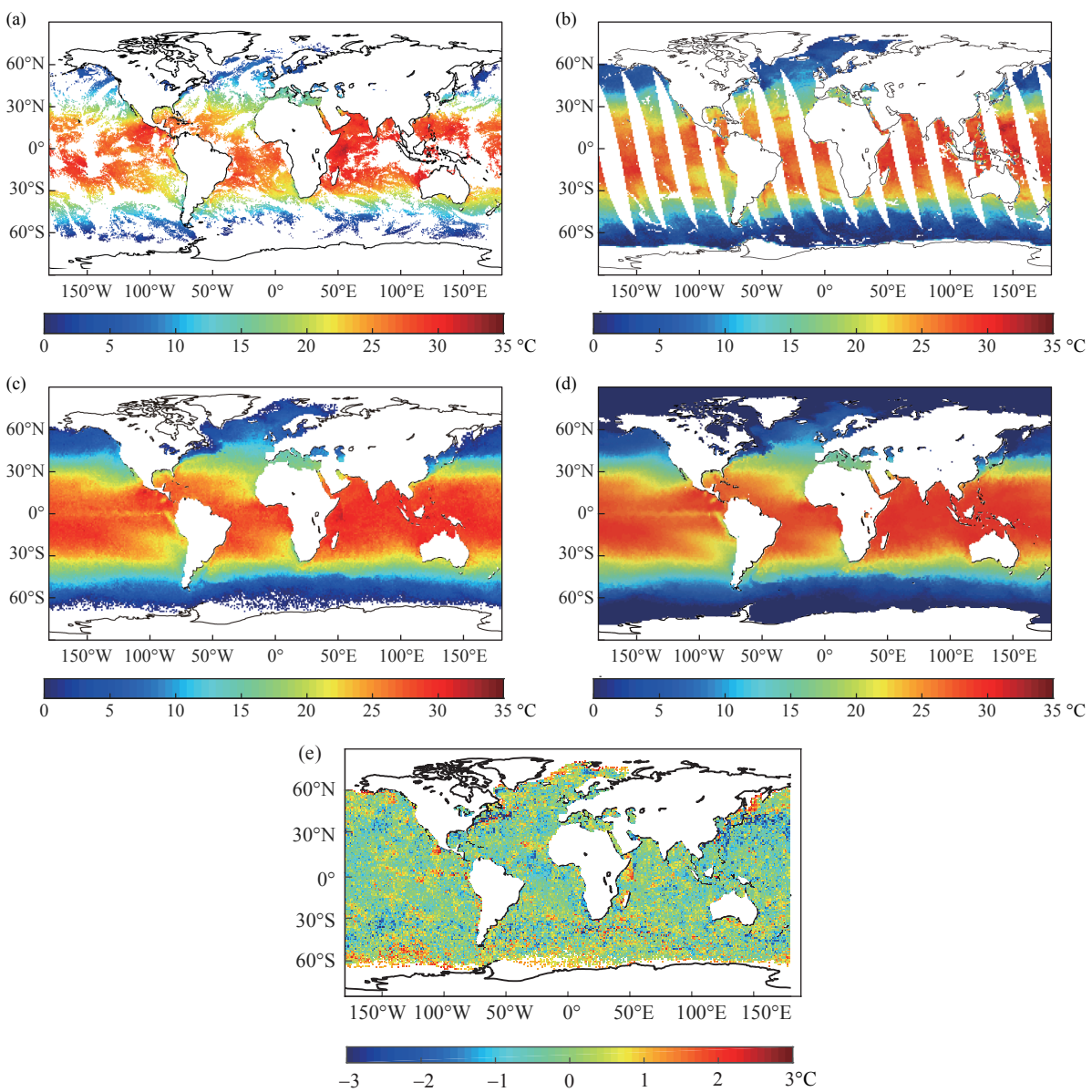

Figure 4. Global distribution of (a) daytime MERSI SST, (b) daytime MWRI SST, (c) fusion SST, (d) OSTIA SST, and (e) difference between fusion SST and OSTIA SST on 3 April, 2021.

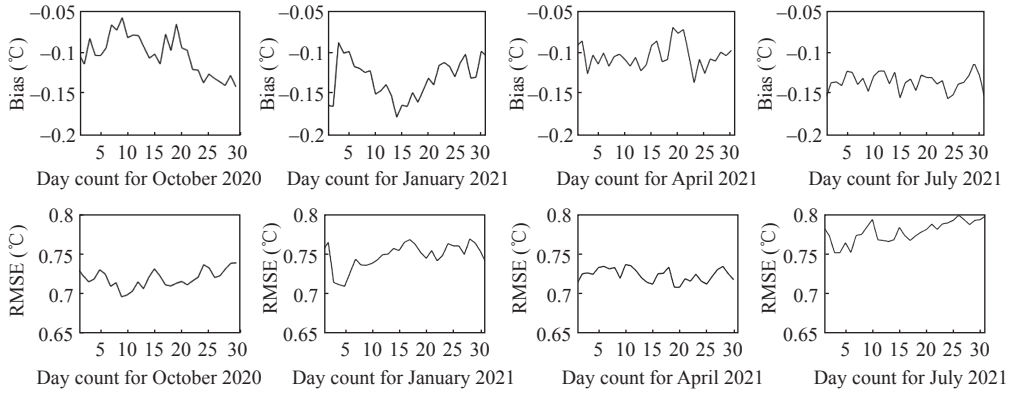

Figure 5. Daily error statistical curve of fusion SST in October 2020, January, April, and July 2021.

Table 1. Error statistical results compared with OSTIA SST.

	Bias (°C)	RMSE (°C)
MERSI daytime SST	0.02	0.72
MERSI nighttime SST	–0.28	0.57
MWRI daytime SST before bias correction	–0.10	0.87
MWRI nighttime SST before bias correction	–0.18	0.91
MWRI daytime SST after bias correction	0.00	0.78
MWRI nighttime SST after bias correction	–0.04	0.79
Fusion SST	–0.12	0.74

5 CONCLUSION AND DISCUSSION

Chinese FY satellites are in urgent need of fusion SST. This paper utilized the OI method to fuse FY-3D/MERSI-II SST and MWRI SST, and conducted quality validation. The conclusions are as follows:

(1) The order of accuracy from high to low is MERSI-II nighttime SST, MERSI-II daytime SST, MWRI daytime SST, and MWRI nighttime SST;

(2) After bias correction, the RMSE of MWRI SST is reduced by about 0.1K compared with that before bias correction;

(3) Data fusion has proven to effectively enhance the spatial coverage of SST, thereby better meeting the requirements of model assimilation and business applications when compared to using solely infrared or microwave SST.

(4) Compared with OSTIA SST, the accuracy of fusion SST is slightly lower than MERSI-II SST and higher than MWRI SST.

The accuracy of fusion SST is highly dependent on the accuracy of MERSI-II SST and MWRI SST. Therefore, further optimization of the retrieval and quality control algorithms of MERSI-II and MWRI SST and optimize the model parameters of fusion algorithms are the key to further improving the accuracy of Chinese FY satellite fusion SST. We will also try to apply artificial intelligence methods to bias correction. In addition, the influence of the diurnal variation of SST [41] is not considered in this paper, and the diurnal variation model will be established later to correct the diurnal variation.

***Acknowledgements*:** We would like to thank WANG Su-juan, LIU Jian and LIAO Zhi-hong for their guidance and support in this work.

REFERENCES

[1] CHEN Y, YAN H M, TAO Y, et al. The relationship between Indian Ocean SST and tropical cyclone genesis frequency over North Indian Ocean in May [J]. Journal of Tropical Meteorology, 2023, 29(3): 359–369, https://doi.org/10.3724/j.1006–8775.2023.027

[2] GUO R Y, PAN W J, KE M L, et al. Diversity on the interannual variations of spring monthly precipitation in southern China and the associated tropical sea surface temperature anomalies [J]. Journal of Tropical Meteorology, 2023, 29(3): 337–346, https://doi.org/10.3724/j.1006–8775.2023.025

[3] LIU Q Q, LI C H, GU D J, et al. Impacts of sea surface temperature on the interannual variability of winter haze days in Guangdong Province [J]. Journal of Tropical Meteorology, 2023, 29(2): 168–178, https://doi.org/10.46267/j.1006–8775.2023.013

[4] DONG N, XU X D, CAI W Y, et al. The response of anomalous vertically integrated moisture flux patterns related to drought and flood in southern China to sea surface temperature anomaly [J]. Journal of Tropical Meteorology, 2023, 29(2): 179–190, https://doi.org/10.46267/j.1006–8775.2023.014

[5] CIANI D, RIO M H, NARDELLI B B, et al. Improving the altimeter-derived surface currents using Sea Surface Temperature (SST) Data: a sensitivity study to SST products [J]. Remote Sensing, 2020, 12(10): 1601, https://doi.org/10.3390/rs12101601

[6] KIM M, YANG H, KIM J. Sea surface temperature and high water temperature occurrence prediction using a long short-term memory model [J]. Remote Sensing, 2020, 12(21): 1–21, https://doi.org/10.3390/rs12213654

[7] BANZON V F, REYNOLDS R W, STOKES D, et al. A 1/4°-spatial-resolution daily sea surface temperature climatology based on a blended satellite and in situ analysis [J]. Journal of Climate, 2014, 27(21): 8221–8228, https://doi.org/10.1175/jcli-d-14–00293.1

[8] LÓPEZ GARCÍA M J. SST Comparison of AVHRR and MODIS time series in the Western Mediterranean Sea [J]. Remote Sensing, 2020, 12: 2241, https://doi.org/10.3390/rs12142241

[9] GANGWAR R K, THAPLIYAL P K. Variational based estimation of sea surface temperature from split window observations of INSAT/3DR Imager [J]. Remote Sensing, 2020, 12(19): 3142, https://doi.org/10.3390/rs12193142
[10] GENTEMANN C L, WENTZ F J, BREWER M, et al. Passive microwave remote sensing of the ocean: an overview [C]// NASA: Oceans from Space Symposium. Venice: 2010.
[11] GENTEMANN C L, WENTZ F J, MEARS C A, et al. In situ validation of tropical rainfall measuring mission microwave sea surface temperatures [J]. Journal of Geophysical Research: Oceans, 2004, 109: C04021, https://doi.org/10.1029/2003JC002092
[12] WENTZ F J, GENTEMANN C, SMITH D, et al. Satellite measurements of sea surface temperature through clouds [J]. Science, 2000, 288: 847–850, https://doi.org/10.1126/science.288.5467.847
[13] BOUALI M, POLITO P S, SATO O T, et al. The impact of cloud masking on the climatology of sea surface temperature gradients [J]. Remote Sensing Letters, 2020, 11(12): 1110–1117, https://doi.org/10.1080/2150704X.2020.1825865
[14] CAO K X, JIN X F, SUN W F, et al. Quality assessment and correction of SST fusion product in the Bohai Sea and the Huanghai Seas [J]. Marine Science, 2017, 41(9): 50–55, in Chinese with English abstract
[15] WENTZ K, MANASTER A. The Microwave Climate Data Center Repository [R]. California: Santa Rosa, 2022, https://doi.org/10.56236/RSS-bh
[16] GOVEKAR P D, GRIFFIN C, BEGGS H. Multi-sensor sea surface temperature products from the Australian Bureau of Meteorology [J]. Remote Sensing, 2022, 14: 3785, https://doi.org/10.3390/rs14153785.
[17] BULGIN C E, MERCHANT C J, FERREIRA D. Tendencies, variability and persistence of sea surface temperature anomalies [J]. Scientific Reports, 2020, 10: 7986, https://doi.org/10.1038/s41598–020–64785–9.
[18] DING R J, ZHAO C F. Study on the merging sea surface temperature data based on optimal interpolation and Bayesian Maximum Entropy Method [J]. Journal of Ocean Technology, 2018, 37 (2): 35–42, in Chinese with English abstract
[19] ZHENG J W, XU D F, XU M Q. A review of merging methods of all covered high resolution SST [J]. Journal of Tropical Oceanography, 2008, 27(4): 77–82, in Chinese with English abstract
[20] REYNOLDS R W, SMITH T M, LIU C, et al. Daily high-resolution-blended analyses for sea surface temperature [J]. Journal of Climate, 2007, 20(22): 5473–5496, https://doi.org/10.1175/2007JCLI1824.1
[21] GEMMILL W. Daily real-time global sea surface temperature: High resolution analysis at NOAA/NCEP [Z]. NOAA/NWS/NCEP/MMAB Office Note, 2007: 260.
[22] GOOD S E, FIEDLER E, MAO C, et al. The current configuration of the OSTIA system for operational production of foundation sea surface temperature and ice concentration analyses [J]. Remote Sensing, 2020, 12(4): 720, https://doi:10.3390/rs12040720
[23] BRASNETT B, COLAN D S. Assimilating retrievals of sea surface temperature from VIIRS and AMSR2 [J]. Journal of Atmospheric and Oceanic Technology, 2016, 33(2): 361–375.
[24] QI Y L, LIN M S. Application of the data fusion technique in HY-2 satellite data [J]. Space Engine, 2012, 21(3): 117–123, in Chinese with English abstract
[25] MIAO C S, CHENG Y, WANG J H, et al. Data fusion of offshore SST from China FY and HY2 satellites and its application [J]. Advance in Earth Science, 2015, 30(10): 1127–1143, in Chinese with English abstract
[26] LIAO Z H. Sea Surface Temperature Reconstruction for FY-3C Satellite Data [D]. Beijing: University of Chinese Academy of Sciences, 2017, in Chinese with English abstract
[27] YANG J, DONG C H, LU N M, et al. FY-3A: The new generation polar-orbiting meteorological satellite of China [J]. Acta Meteorologica Sinica, 2009, 67(4): 501–509, https://doi.org/10.11676/qxxb2009.050
[28] ZHANG P, LU Q F, HU X Q, et al. Latest progress of the Chinese meteorological satellite program and core data processing technologies [J]. Advances in Atmospheric Sciences, 2019, 36(9): 1027–1045, https://doi.org/10.1007/s00376–019–8215-x
[29] WANG S J, CUI P, ZHANG P, et al. FY-3C/VIRR sea surface temperature products and quality validation [J]. Journal of Applied Meteorology, 2020, 31(6): 729–739, in Chinese with English abstract
[30] ZHANG H, IGNATOV A, HINSHAW D. Evaluation of the in situ Sea Surface Temperature Quality Control in the NOAA in situ SST Quality Monitor (*i*Quam) System [J]. Journal of Atmospheric and Oceanic Technology, 2021, 38(7): 1249-1263, https://doi.org/10.1175/JTECH-D-20–0203.1
[31] MERCHANT C. Quick Start Guide to ESA SST CCI Products [R]. York Shire: Reading, ESA, 2013.
[32] ZHANG M, WANG S J, QIN D Y, et al. The inversion and quality validation of FY-3C MWRI sea surface temperature [J]. Journal of Remote Sensing, 2018, 22(5): 713–722, https://doi.org/10.11834/jrs.20187217, in Chinese with English abstract
[33] WENTZ F J, MEISSNER T. Supplement 1 Algorithm Theoretical Basis Document for AMSR-E Ocean Algorithms [R]. California: Santa Rosa, NASA, 2007.
[34] MENG X. Merging Infrared Radiometer and Microwave Radiometer Sea Surface Temperature Data Based on the Optimum Interpolation [D]. Beijing: National Marine Environment Prediction Research Center, 2011, in Chinese with English abstract
[35] YANG C, LEONELLI F E, MARULLO S, et al. Sea Surface Temperature Intercomparison in the Framework of the Copernicus Climate Change Service (C3S) [J]. Journal of Climate, 2021, 34(13): 5257-5283, https://doi.org/10.1175/JCLI-D-20–0793.1
[36] HU X R, HAN Z, LI J, et al. Regional sea surface temperature data fusion based on ensemble Kalman filter [J]. Advances in Marine Science, 2018, 36(3): 394–401 (in Chinese).
[37] ZHANG Y X, LI X, ZHANG M, et al. On-orbit radiometric calibration for thermal infrared band of FY3D/MERSI-II satellite remote sensor based on Qinghai Lake radiation calibration test-site [J]. Acta Photonica Sinica, 2020, 49(5): 0528002.
[38] ZENG Z Q, JIANG G M. Intercalibration of the Microwave Radiation Imager on Fengyun 3C [J]. Remote Sensing Technology and Application, 2021, 36(3): 682–691, in Chinese with English abstract.

[39] GENTEMANN C L, MEISSNER T, WENTZ F J. Accuracy of satellite sea surface temperatures at 7 and 11 GHz [J]. IEEE Transactions on Geoscience and Remote Sensing, 2010, 48(3): 1009–1018, https://doi.org/10.1109/TGRS.2009.2030322

[40] ZHANG M, SUN F L, DOU F L, et al. Improving the FY-3D MWRI sea surface temperature based on simulated 6.9 GHz brightness temperature [J]. Meteorological Science and Technology, 2022, 50(2): 189–193, in Chinese with English abstract

[41] GENTEMANN C L, DONLON C J, STUART-MENTETH A, et al. Diurnal signals in satellite sea surface temperature measurements [J]. Geophysical Research Letters, 2003, 30(3): 1140, https://doi.org/10.1029/2002GL016291

Citation: ZHANG Miao, XU Na, CHEN Lin. Fusion SST from Infrared and Microwave Measurement of FY-3D Meteorological Satellite [J]. Journal of Tropical Meteorology, 2024, 30(1): 89-96, https://doi.org/10.3724/j.1006-8775.2024.009